Exhumational history of the north central Pamir

William H. Amidon[1] and Scott A. Hynek[2]

Received 3 August 2009; revised 7 June 2010; accepted 21 June 2010; published 12 October 2010.

[1] The Pamir plateau forms a prominent tectonic salient along the western end of the Tibet-Tarim margin. Despite its tectonic significance, relatively little is known about the timing of major Cenozoic tectonic events in the Pamir. Here we present new apatite and zircon (U/Th)-He ages, bulk rock geochemistry, and Al-in-hornblende barometry results from the Karakul graben, a prominent north-south oriented rift basin located ~50 km south of the Main Pamir Thrust. Although cooling ages do not record the onset of extension, graben-bounding normal faults provide exposures of otherwise slowly eroding rocks which record two Cenozoic thermal events. Existing geochronology and new results suggest that granitic rocks in the Karakul region were shallowly emplaced, cooled very quickly through ~300°C, and have experienced less than 10 km of exhumation since the late Triassic. A long period of relatively slow exhumation throughout much of the late Mesozoic and Cenozoic was punctuated by two periods of accelerated exhumation during the middle Eocene (~50–40 Ma) and early Miocene (~25–16 Ma). We interpret the first period of accelerated exhumation as a result of tectonic uplift and subsequent erosion due to the northward propagation of the India-Asia collision. We attribute the second period of rapid exhumation to a renewed phase of tectonism and plateau uplift in the Pamir, perhaps related to a break off event along the down-going Indian plate at ~25 Ma or to the onset of slip along the nascent Karakoram fault. **Citation:** Amidon, W. H., and S. A. Hynek (2010), Exhumational history of the north central Pamir, *Tectonics*, *29*, TC5017, doi:10.1029/2009TC002589.

1. Introduction

[2] The Tibetan plateau is flanked by active orogens along both its northern and southern margins. Along the southern margin India-Asia convergence is accommodated by the thrust sheets of the Himalayan chain, and to the north by a more disparate series of mountain belts including the Qilian Shan, Kunlun Shan, Tien Shan, and Pamir. Although this deformation is clearly the result of India-Asia collision, several different models have been proposed for northward propagation of active deformation. In the stepwise growth model, India-Asia convergence propagates northward by slip along successively activated thrust and strike slip faults [*Tapponnier et al.*, 2001]. In viscous sheet models, the lithosphere deforms as a continuous medium, with thickening and strain rates initially highest in the south, and gradually increasing toward the north [*Clark and Royden*, 2000; *England and Houseman*, 1986]. Although both of these models predict a time-dependent south to north migration of tectonic uplift, an increasing body of evidence suggests that tectonic thickening along the northern margin of Tibet commenced soon after India-Asia collision, and has continued in a complex pattern since that time [*Wang et al.*, 2006; *Yin et al.*, 2008; *Zhu et al.*, 2006]. Understanding the history of far field deformation related to the India-Asia collision may provide a valuable analog for the cycle of mountain building and erosion throughout Earth's history and on other planets.

[3] The Pamir mountains lie along the western end of the Tibet-Tarim margin, where as much as 200–400 km of Eurasian crust may have been subducted beneath the encroaching Pamir [*Burtman*, 2000; *Burtman and Molnar*, 1993]. Today, ~8–23 mm/yr of India-Asia convergence is accommodated across a relatively narrow zone of north vergent thrust faulting [*Arrowsmith and Strecker*, 1999; *Reigber et al.*, 2001; *Strecker et al.*, 2003]. In map view, the Pamir creates a prominent arc, often referred to as an orocline, which mimics the shape of the western Himalayan syntaxis immediately to its south. A variety of ideas have been put forward to understand how this arc-shaped tectonic feature has evolved and its implications for deformation of the western Tibetan plateau. Early studies suggested that the Pamir developed in part by large offsets on the Karakoram fault, which transferred strain to E–W oriented thrust faults within and at the margins of the Pamir [*Peltzer and Tapponnier*, 1988]. Subsequent ideas require more moderate offsets on the Karakoram, and include elements of radial thrusting, oroclinal bending, block rotation, and extensional faulting [*Robinson*, 2009; *Robinson et al.*, 2004; *Strecker et al.*, 1995; *Yin et al.*, 2001]. The timing of extension within the Pamir is of particular interest as it remains unclear whether extension is in response to crustal thickening [*Brunel et al.*, 1994], radial thrusting [*Strecker et al.*, 1995], oroclinal bending [*Yin et al.*, 2001], or asymmetric overthrusting of the Pamir to the northwest [*Cowgill*, 2010]. Answering these questions, and relating the timing and style of mountain building in the Pamir to the rest of the Indo-Himalayan orogen requires a basic chronology of when Cenozoic deformation began within and around the margins of the Pamir salient.

[1]Department of Geology, Middlebury College, Middlebury, Vermont, USA.
[2]Department of Geology and Geophysics, University of Utah, Salt Lake City, Utah, USA.

0278-7407/10/2009TC002589

[4] The Karakul basin is one of the most prominent physiographic features of the northern Pamir. Although originally mapped as an extensional graben [*Noth*, 1932], subsequent workers have proposed that the basin is an impact structure [*Gurov et al.*, 1993]. Several recent studies, including this one, conclude that the basin is in fact a graben and is currently experiencing NW–SE directed transtensional deformation [*Blisniuk and Strecker*, 1997; *Strecker et al.*, 1995]. We present new apatite and zircon (U/Th)-He cooling ages in an effort to document the exhumational history of the Karakul region and relate it to Cenozoic tectonic uplift and/or extension within the Pamir plateau. Although cooling ages do not record the onset of extension, graben-bounding normal faults provide exposures of otherwise slowly eroding rocks which appear to record two Cenozoic thermal events. Relatively slow cooling since ~220 Ma is punctuated by two episodes of more rapid cooling and exhumation between ~50–40 Ma and ~25–16 Ma. We interpret the first period of accelerated exhumation as an erosional response to tectonic uplift associated with the early stages of the India-Asia collision. We argue that the second period of accelerated exhumation is part of a regional uplift event, likely reflecting accelerated rates of tectonic convergence and crustal thickening throughout the Pamir and Tien Shan.

2. Geological Setting

2.1. Regional Geology

[5] The Pamir mountains are composed of Paleozoic-Mesozoic accreted terranes that are deflected northward from their continuations across Afghanistan and Tibet [*Burtman and Molnar*, 1993; *Tapponnier et al.*, 1981; *Yin and Harrison*, 2000]. The Karakul granites are part of the Northern Pamir terrane, which likely correlates with the Songpan-Garze terrane in Tibet [*Robinson*, 2009; *Schwab et al.*, 2004; *Yin and Harrison*, 2000]. This correlation is most convincingly supported by the data of *Schwab et al.* [2004], who identify a continuous chain of ~200 Ma plutons with similar geochemical characteristics wrapping around the Pamir from the Karakul basin, through the Muji basin and into the Mazar region of the western Kunlun (Figure 1). Based on bulk rock geochemistry, they divide these late Jurassic plutons into the Kunlun magmatic arc (north of the Kunlun suture), and the Karakul-Mazar belt (south of the Kunlun suture).

[6] Late Cenozoic tectonics of the eastern Pamir (Figure 1) are dominated by (1) internal crustal thickening and northward thrusting of the Pamir-Alai range over the Eurasian continent along the Main Pamir Thrust (MPT), (2) strike-slip motion along the northern extension of the Karakoram fault system, and (3) east–west extension along the Kongur Shan extensional systems. The MPT is a complex structural feature, which probably originated as a Paleozoic suture and may have experienced several episodes of shortening since that time [*Burtman and Molnar*, 1993]. Accelerated Cenozoic tectonic activity along the MPT is recorded by reset apatite fission track ages in basinal sediments reflecting rapid exhumation between ~22–17 Ma along the Kumtag thrust [*Sobel and Dumitru*, 1997]. Renewed activity in the latest Oligocene or early Miocene is also recorded by the sedimentary deposits in the Alai valley and Tajik depression, which show an increase in terrestrial clastic sedimentation and accelerated basin subsidence at this time [*Coutand et al.*, 2002; *Leith*, 1985]. A large amount of displacement has clearly been accommodated across the MPT zone, yet the degree of internal shortening within the plateau interior is poorly documented. Little evidence exists for active Cenozoic thrust faulting within the northern and central Pamir, but Cenozoic thrusting within the southern Pamir may have been significant, particularly along faults bounding the Rushan-Pshart zone [*Burtman and Molnar*, 1993; *Schmalholz*, 2004].

[7] Although the chronology of Cenozoic shortening within the Pamir is poorly known, a portion of it must have been kinematically linked to right-lateral slip along the Karakoram fault system. The Karakoram fault has partially accommodated northward indentation of the western Himalayan syntaxis, feeding some fraction of this displacement into the Rushan-Pshart zone [*Burtman and Molnar*, 1993; *Robinson*, 2009; *Strecker et al.*, 1995]. Considerable debate has focused around the timing of initiation along of the Karakoram fault, with estimates ranging from <13 Ma [*Murphy et al.*, 2000], to 13–15 Ma [*Phillips et al.*, 2004], and 25–22 Ma [*Lacassin et al.*, 2004; *Valli et al.*, 2008]. Offsets of the Aghil limestone suggest a total displacement of ~160 km along the northern section of the Karakoram [*Robinson*, 2009].

[8] Formation of the Karakul graben may be related temporally and/or mechanically to extension along the Kongur Shan fault system or to the unroofing of gneiss domes within the central and eastern Pamir. The Kongur Shan extensional system comprises a series of north–south oriented normal faults that accommodate east–west extension along the eastern margin of the Pamir plateau. Near its southern end the Kongur Shan fault system bounds the Muztagh-Ata gneiss dome [*Robinson et al.*, 2007]. It appears that a period of crustal thickening occurred during the late Oligocene and early Miocene, which culminated in extrusion of the Muztagh-Ata dome during the middle Miocene. Thickening and subsequent extrusion of the Muztagh-Ata gneiss dome is thought to have occurred along a lower crustal detachment referred to as the eastern Pamir shear zone [*Robinson et al.*, 2007]. A similar history is inferred for the central Pamir gneiss domes (the Sares and Muzkol domes shown in Figure 1), although these appear to have begun exhumation during the latest Oligocene or early Miocene [*Robinson et al.*, 2007; *Schmalholz*, 2004]. The onset of east–west extension along the Kongur Shan fault system is interpreted to postdate extrusion of the gneiss domes, beginning in the late Miocene at ~7–8 Ma [*Robinson et al.*, 2004].

2.2. Previous Work in the Karakul Region

[9] The Karakul basin is a ~50 km wide depression bounded by steep north–south oriented flanks with a maximum relief of ~1500 m (Figure 2). The basin sits atop ~70–75 km thick crust, whose uppermost section is composed of strongly folded and faulted Paleozoic metasediments intru-

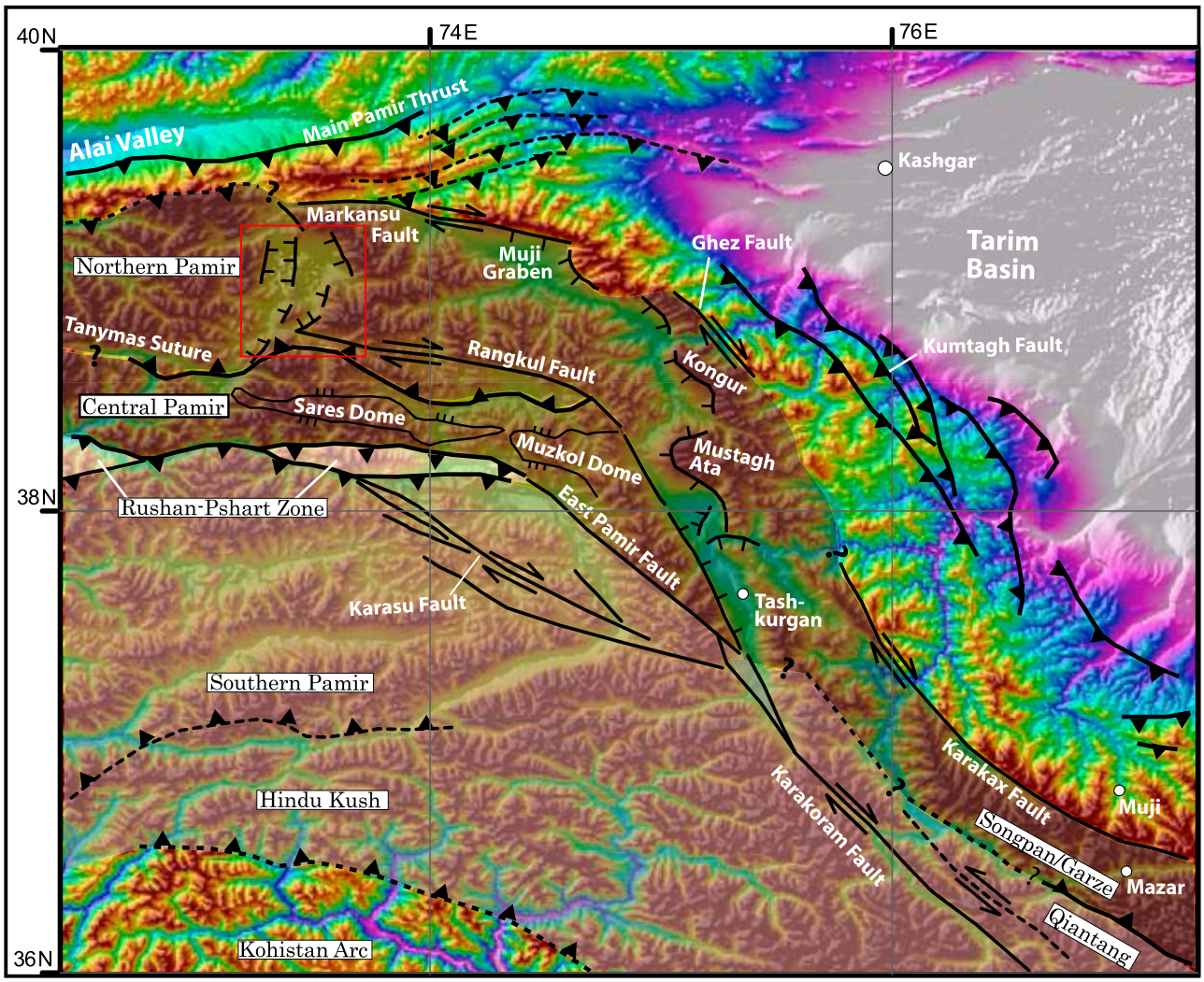

Figure 1. Map showing the regional tectonics of the Pamir Plateau and Tarim Basin, synthesized from *Matte et al.* [1996], *Burtman and Molnar* [1993], *Searle* [1996], *Raterman et al.* [2007], and *Robinson* [2009].

ded by latest Triassic granodiorites [*Beloussov et al.*, 1980; *Burtman and Molnar*, 1993]. The lake itself has two lobes separated by a central island and peninsula, reaching depths of >230 m in the western lobe and only ~30 m in the eastern lobe [*Noth*, 1932]. Quaternary normal fault scarps in the northern and southern parts of the basin have been mapped in detail and provide evidence that the basin is an extensional graben [*Blisniuk and Strecker*, 1996, 1997; *Strecker et al.*, 1995]. It has been suggested that the central island and peninsula constitute a central horst structure, and that the principal bounding fault is on the western flank of the basin with a throw of at least 1200 m [*Strecker et al.*, 1995]. Holocene normal fault scarps have been documented in the northern and southern ends of the lake basin. The scarps are typically quite high angle (~60°), and are dominantly oriented N–S near the northern part of the lake, and NE–SW in the south. Kinematic indicators compiled from individual slip surfaces on each scarp suggest right lateral oblique extension across the basin, with a mean extensional direction of 132 ± 4° [*Blisniuk and Strecker*, 1997].

[10] The observed normal faults record at least 3 generations of faulting, the youngest of which is recorded by scarps in the modern braid plain of the Muzkol River [*Strecker et al.*, 1995]. Although no absolute chronologies have been established for the older offsets, some scarps cut highly weathered terminal moraines which have been suggested to be at least ~120 ka old [*Komatsu et al.*, 2010]. Because the largest and oldest scarps do not typically exceed ~30 m in height, and are likely cutting surfaces >100 ka in age, the current rate of extension across the Karakul graben is unlikely to exceed about 1 mm/yr. Although no constraints exist on the initiation of extensional faulting, the potentially slow rate of extension and the highly incised flanks of the graben suggest that the onset of faulting must

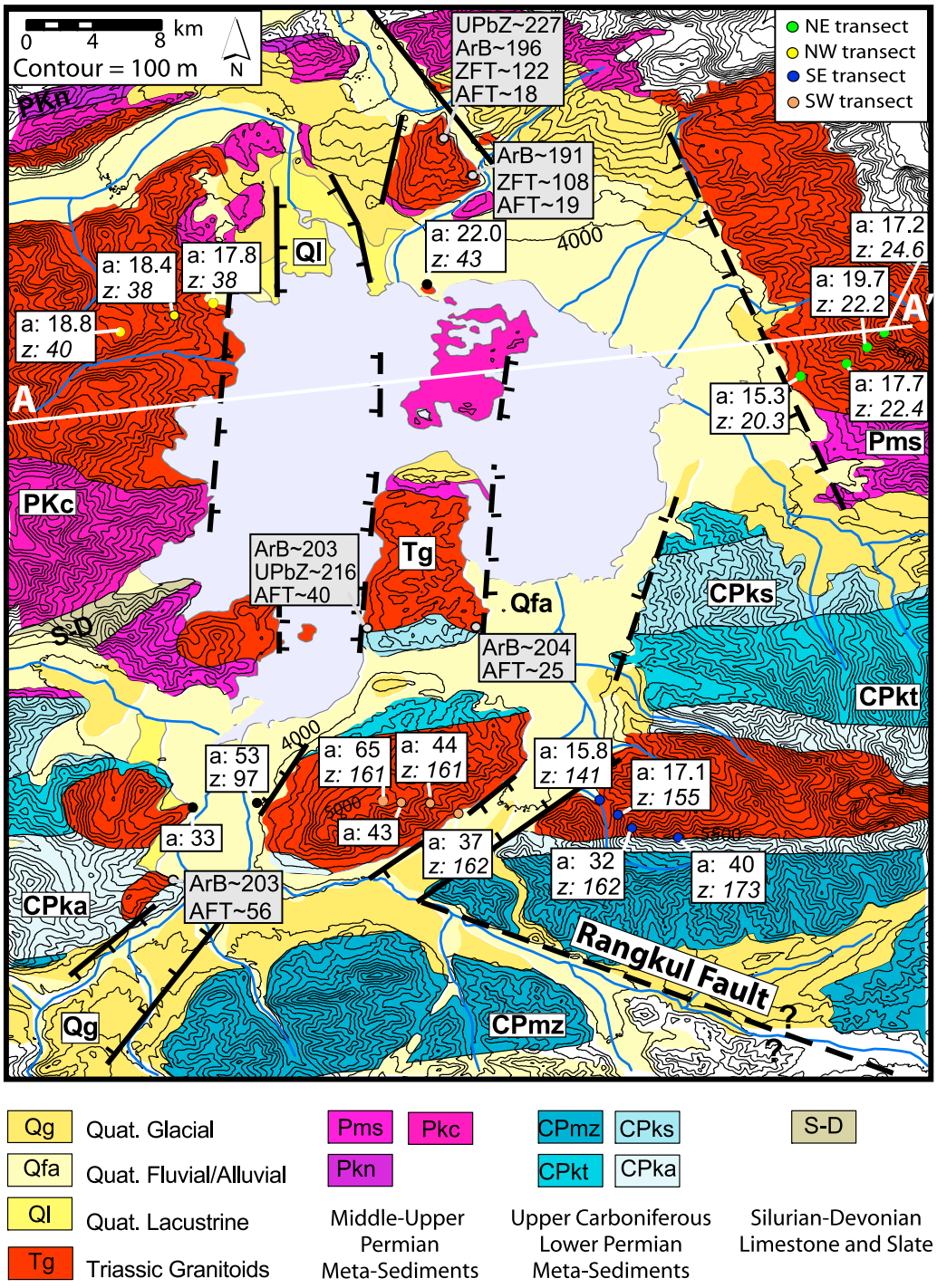

Figure 2. Geologic map of the Karakul basin. Bedrock geology is taken from *Romanko* [1968]. Structures are from field observations, interpretations of satellite imagery, and the observations of *Blisniuk and Strecker* [1997]. White boxes contain mean apatite ("a") or zircon ("z") (U/Th)-He ages. Gray boxes show results from *Schmalholz* [2004] including biotite $^{40}Ar/^{39}Ar$ ages ("ArB"), zircon U-Pb ages ("UPbZ"), and apatite and zircon fission track ages (AFT and ZFT). Hatched lines are normal faults, dashed lines are hypothesized, and solid lines are where scarps are observed.

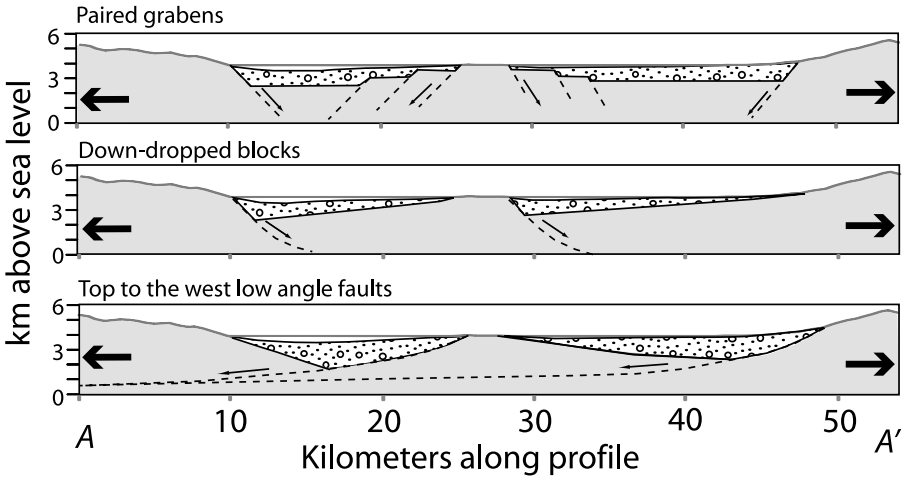

Figure 3. Topographic profile across the Karakul basin derived from 90 m SRTM digital elevation data (thick gray line). (top) Our preferred structural geometry of paired grabens bound by relatively high angle normal faults. (middle and bottom) Alternative structural interpretations.

have begun at least several million years ago and likely earlier.

[11] Although several previous studies have inferred plausible geometries for basin-bounding normal faults, significant uncertainty remains. Because the interpretation of (U/Th)-He cooling ages hinges on the assumed structural geometry, it is worth discussion here. The steep relief and deep basin along the western flank led *Strecker et al.* [1995] to identify this as the master extensional fault. Although the eastern flank of the graben has the sharp linear characteristics of a large normal fault, its lack of fault scarps, sediment laden footwall, and shallow lake basin all suggest that it has either experienced a lower magnitude of Quaternary slip or much higher volume of sediment production. Figure 3 depicts a topographic profile derived from 90 m SRTM data with sketches of three possible fault geometries: (1) a pair of grabens bounded by high-angle normal faults, (2) a pair of crustal blocks down-dropped along top to the east faults, and (3) a system of low-angle top to the west normal faults. Based on the high angle and linear trace of observed fault scarps, as well as the existence of eastward facing fault scarps at both the northern and southern ends of the lake [*Blisniuk and Strecker*, 1997], we prefer the paired graben model and base the rest of our analysis on this structural model.

[12] Existing thermochronology from the Karakul basin is summarized in Figure 2, and includes many U-Pb zircon crystallization ages, several biotite $^{40}Ar/^{39}Ar$ cooling ages, as well as zircon and apatite fission track ages [*Schmalholz*, 2004; *Schwab et al.*, 1999]. Zircon U-Pb ages were derived from multiple ID-TIMS and SHRIMP analyses of zircons from two sites. A range of discordant and concordant behavior was observed, ultimately leading the authors to conclude that the batholiths in the Karakul area crystallized over a time span from 225 to 200 Ma. In contrast, $^{40}Ar/^{49}Ar$ age spectra from muscovite and biotite show no evidence of thermal disturbance and give consistent calculated age ranges of 207 to 191 Ma. Due to their similarity with the zircon ages these $^{40}Ar/^{49}Ar$ ages are interpreted to reflect pluton emplacement and very early cooling. Two zircon fission track ages from the northern end of the lake give apparent ages of 108 and 122 Ma and are thought to reflect slow denudational cooling following granitoid emplacement. Apatite fission track ages decrease from ~56 Ma in the south to ~18 Ma in the north. *Schmalholz* [2004] tentatively explains the south to north younging of fission track ages as a response to out of sequence thrusting on the proto-Markansu fault, suggesting that the Karakul region behaved as a rigid tectonic block during this tectonism. It is also noted that none of the fission track ages provide conclusive evidence for the onset of extensional faulting within the Karakul graben [*Schmalholz*, 2004].

3. Methods

[13] Samples were collected from four vertical transects of granodiorites containing plagioclase > quartz > biotite ± K-feldspar ± muscovite, with abundant zircon, apatite, epidote and titanite occurring as accessory phases. The petrology of the NE profile differs significantly from the others, and is presented in Table S3.[1] Sample TAJ93 from the NE profile is a hornblende-diorite, whereas samples TAJ96 and TAJ102 are garnet bearing granodiorites with garnets >1 cm present in sample TAJ96. For all samples, inclusion-free apatites and zircons were handpicked, and measured in all three dimensions. Alpha ejection correction factors [*Farley et al.*, 1996] were computed from length and mean width. Apatites were analyzed for He, U, and Th following published procedures [*House et al.*, 2000]. Zircons were degassed for helium

[1] Auxiliary materials are available in the HTML. doi:10.1029/2009TC002589.

Table 1. U/Th-He Cooling Ages[a]

Sample	Latitude[b]	Longitude[b]	Elevation (m asl)	Apatite (Ma)	Zircon (Ma)
		NE Transect			
taj-93	39.1010	73.6730	5579	17.2	24.6
taj-96	39.0934	73.6638	5094	19.1	22.2
taj-99	39.0846	73.6525	4663	17.7	22.4
taj-102	39.0776	73.6280	4212	15.3	21.0
		SW Transect			
P916-1	38.8456	73.4178	4654	43.0	—
P916-2	38.8445	73.3942	5069	64.6	164.9
P916-3	38.8431	73.4198	4560	44.3	161.1
P916-4	38.8377	73.4348	4098	37.2	162.2
		SE Transect			
P917-1	38.8247	73.5567	5465	39.8	172.7
P917-2	38.8298	73.5323	4900	31.5	162.2
P917-3	38.8373	73.5244	4497	17.1	154.9
P917-4	38.8451	73.5147	4112	15.4	139.4
		NW Transect			
P919-1	39.1193	73.3018	3929	17.8	37.8
P919-2	39.1019	73.2496	4915	18.8	39.7
P919-3	39.1100	73.2812	4423	18.4	38.0
		Lake Level			
P918-1[c]	38.8402	73.3243	3947	69.9	96.5
P918-2	38.8429	73.2912	3950	32.9	—
P919-1a	39.1263	73.4203	3937	22.0	42.6
		Standards			
Durango	—	—	—	32.5	—
FCT	—	—	—	—	27.7

[a]Here asl, above sea level; 1σ errors are ~7% for both apatite and zircon.
[b]World Geodetic System 84.
[c]Poor reproducibility of apatite ages, 1σ error ~30%.

analysis by lasing inside of sapphire microfurnaces with removable cover pieces for easy removal of grains following lasing. The microfurnaces were heated to ~1510°C for 12 min, and helium reextracts typically yielded <1% of the primary extraction. Helium blanks were consistently less than 0.1% of sample concentrations for apatite, and even less for zircon. Zircons were then transferred into Parr bomb capsules and spiked for measurement of U and Th by isotope dilution. Parr bomb dissolution proceeded by dissolving samples in HF at 220°C for 48 h, drying down and redissolving in 6 N HCL for 24 h, followed by a final dry down and redissolution in a 5% nitric acid solution for ICP-MS analysis. Blanks achieved by this method were typically ~3 pg of U and ~20 pg of Th, representing <0.1% of measured U and <3% of measured Th in all samples. Seven replicate analyses, each consisting of multiple Durango apatite grains yielded a mean age of 32.5 ± 1 Ma [*Farley*, 2000; *Young et al.*, 1969]. Three replicate analyses of single zircon grains from the Fish Canyon tuff yielded a mean age of 27.7 ± 1.5 Ma [*Reiners et al.*, 2002; *Renne et al.*, 1994]. Data are available in Tables S1 and S2.

[14] Compositional analyses on mineral phases were made on polished rock sections using the JEOL JXA-8200 electron microprobe at Caltech. Bulk rock geochemical analyses were made at Michigan State University on samples from three different profiles, as well as a fourth sample from a basaltic dike (sample P916-1). For each profile a fist-sized piece of rock was taken from each sample, amalgamated by powdering and then fused into a glass disk. Major element analyses were made with a Bruker S4 Pioneer XRF, whereas trace elements and REEs were analyzed by LA-ICP-MS using a 266 nm Nd:YAG laser coupled to a Micromass ICP-MS.

4. Results

[15] Single grain apatite and zircon (U/Th)-He ages are presented from all four vertical transects, and from three additional sites near lake level (Table 1, Figure 4, and Tables S1 and S2). Ages are calculated following the standard age equation, including decay of Sm for apatite, but not for zircon. Ages are adjusted for alpha ejection using FT factors calculated following *Farley et al.* [1996], which ranged from 0.77 to 0.85 for apatite and 0.8–0.9 for zircon. Because only ~3 individual grain analyses were performed per sample, it is difficult to assign an external reproducibility for each sample. Instead, we determine a single standard deviation for the entire population by normalizing each analysis by its mean sample age. This procedure gives ~7% standard deviation for both apatite and zircon analyses, which we adopt as the uncertainty on all ages. One major exception are six apatite analyses from sample P918-1, which reproduce very poorly and are not included in the population-wide standard deviation. Interestingly, this is the only sample that exhibits a shear fabric, suggesting that the poor reproducibility could be due to thermal disturbance, microinclusions, or lattice damage acquired during shearing. Two additional analyses P919-3a (apatite) and P916-4c (zircon) are also assumed to be outliers and are included in the population-wide standard deviation, but not in their respective sample means.

[16] Our youngest apatite ages cluster between ~19–15 Ma, and are obtained on the two northern profiles, as well as the bottom of the SE profile (Figure 4 and Table 1). All apatite ages on the two northern profiles are within 2σ error of the other ages from the same profile. Another group of apatite ages cluster between ~44–33 Ma, observed in samples from the southern part of the lake. Zircon ages can be divided into three groups: (1) 25–21 Ma ages observed along the northeastern profile, (2) 40–38 Ma ages along the northwestern profile, and (3) mostly ~165–150 Ma ages in the southern part of the lake. All zircon ages along the northwestern profile are also within 2σ error of each other.

[17] Mineral compositions from the NE transect (Table S3) were analyzed in an effort to estimate the pressure and temperature of pluton emplacement. Compositional profiles across garnet-biotite grain boundaries show highly elevated Mn and depleted Mg concentrations near garnet rims, suggesting that they were altered during retrograde diffusion, or were incorporated from mafic schists in the wall rock [*Kohn and Spear*, 2000]. Garnet-biotite temperature estimates for samples TAJ93 and TAJ102 do not converge on reasonable results and are not discussed further. Sample TAJ93 contains abundant hornblende, as well as a K-feldspar, plagioclase, ilmenite, titanite and epidote mineral assemblage, ideal for Al-in-hornblende barometry [*Hammarstrom and Zen*, 1986;

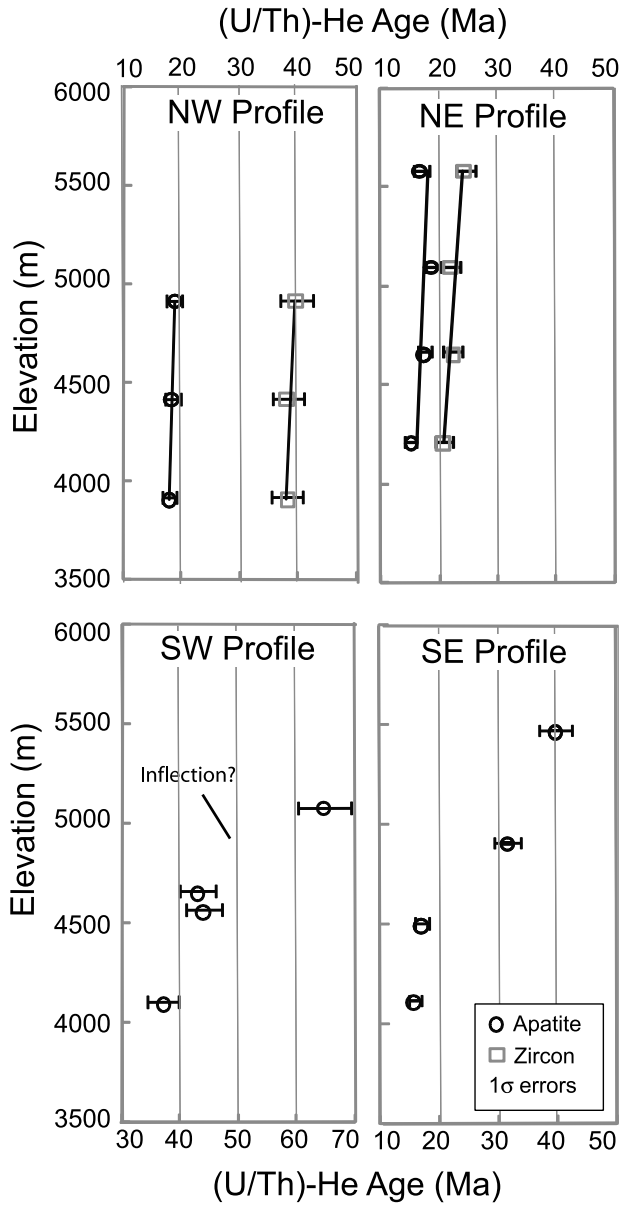

Figure 4. Age-elevation profiles from each of the four transects shown in Figure 2. All errors are 1σ and are ~7% for both apatite and zircon. Note the time scale on the SW profile spans 30 to 70 Ma rather than 10 to 50 Ma. Data are available in Tables S1 and S2.

Hollister et al., 1987]. The cores of ~120 different hornblende grains were analyzed and a plot of Al versus Fe/(Fe+Mg) was used to assess the possibility of low-temperature alteration (Figure S1). This plot shows a positive linear relationship indicating alteration in some grains. To best approximate an unaltered composition, we base our Al-in-hornblende pressure calculations on the average composition of the quartile of analyses containing the highest Al contents and Fe/(Fe+Mg) ratios, as shown in Figure S1. Mineral compositions are presented in Table S3 and yield emplacement pressures of ~2.3 ± 0.5 Kb using the Probe-Amph program [*Tindle and Webb*, 1994].

[18] Bulk rock geochemistry provides a comparison between the Karakul granodiorites and their probable counterparts in the western Kunlun region. Results presented in Figure 5 and in Table S4 show that samples P916, P917, and P919 all have typical granodiorite compositions, whereas the mafic dike from the SW transect (sample P916-1) has an alkaline basalt composition. The total REE content of the granodiorites is quite low (~150–200 ppm), characterized by moderate LREE enrichment (LREE/HREE = 3.5–6.5) and a weak Eu anomaly. Comparison of our data with plutons from the north and south Kunlun belts [*Yuan et al.*, 2002; *Yuquan et al.*, 1996], as well as that of *Schwab et al.* [2004], supports the idea that the Karakul granites are correlative with the Mazar granites, and are slightly different from granites of similar age north of the Kunlun suture. The REE pattern from the Karakul granites is virtually identical to the Mazar granodiorite, but has notably lower concentrations of HREE's than the Arkarz Intrusive Complex (ARIC) that occurs north of the Kunlun suture near Kudi [*Yuan et al.*, 2002]. Trace element data further support this correlation, providing a nearly identical match between the Mazar granodiorite and the Karakul granites.

5. Interpretation of Thermal History

[19] In the following discussion, we use (U/Th)-He ages in two ways: (1) we compare pairs of zircon and apatite ages from the same sample, and (2) we compare age-elevation plots (vertical transects) of apatite or zircon ages. The goal of the first approach is to exploit the difference in closure temperature between zircon (~180°C) and apatite (~65°C) to constrain how long it took for a given sample to cool between these two temperatures [*Farley*, 2002; *Reiners et al.*, 2004]. However, because different thermal histories can produce identical ages in a given crystal, it is necessary to interpret these paired thermochronometers using a time-temperature-age model such as the HeFTy program [*Ketcham*, 2005]. When using HeFTy, we adopt the He diffusion kinetics of *Farley* [2000] for apatite and those of *Reiners et al.* [2004] for zircon. In the second approach (vertical transects), samples are collected along the steepest possible slopes (ideally along fault scarps), under the assumption that these approximate a vertical slice into a laterally homogenous crust. The slope of a line in age versus elevation space can then be used to directly infer the vertical exhumation rate if it is assumed that (1) the closure temperature was the same for all samples in the transect, (2) the thermal gradient was constant during the period considered, and (3) the block has not been significantly tilted [*Ehlers and Farley*, 2003; *Stockli et al.*, 2003]. The second assumption is reasonable because our Al-hornblende barometries and old zircon (U/Th)-He results suggest that exhumation was slow until the onset of exhumation in the mid-Cenozoic. To compare exhumation rates inferred from vertical transects with cooling rates from our paired apatite and zircon ages, we assume a thermal gradient of 25°C/km.

[20] Several lines of evidence suggest that the Karakul granites cooled quickly following their emplacement in the latest Triassic, and then cooled very slowly through the late Jurassic and Cretaceous periods. For example, the short time

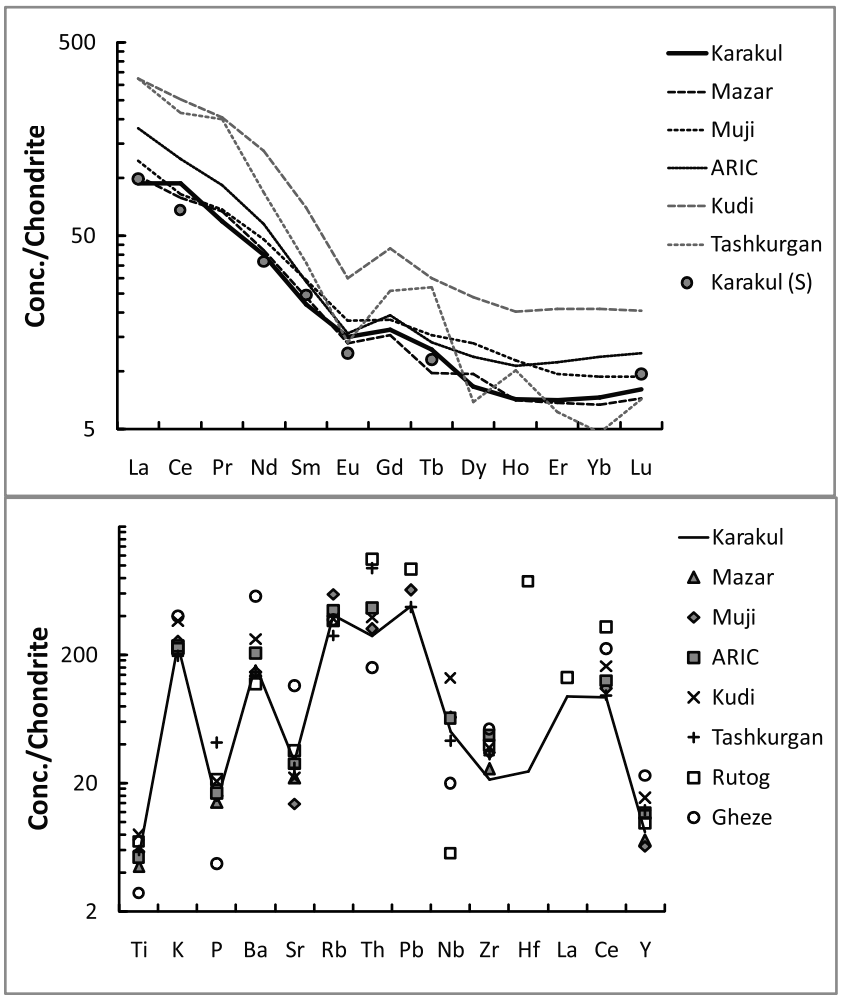

Figure 5. Comparison of the average (top) REE and (bottom) trace element distributions for the Karakul granodiorites to other granitoids in western Tibet. The Karakul granodiorites are nearly identical to that of the Mazar granodiorite and only slightly different from the Arkarz Shan Intrusive Complex (ARIC) near Kudi [*Yuan et al.*, 2002] and from the Muji granitoids [*Yuquan et al.*, 1996]. Solid circles in Figure 5 (top) show previously published data from the Karakul granites [*Schwab et al.*, 2004]. Data from granitoids elsewhere in Tibet are shown for comparison and is taken from *Yuquan et al.* [1996]. The Karakul, Muji, Mazar, and ARIC granites are ~200–230 Ma, whereas Rutog, Gheze, and Tashkurgan are <100 Ma, and Kudi is ~380 Ma.

between zircon crystallization ages (~220 Ma) and biotite $^{40}Ar/^{39}Ar$ cooling ages (~203 Ma) in the southern part of the lake [*Schwab et al.*, 2004], suggests that the Karakul granites were emplaced at relatively shallow depths and cooled quickly through ~300°C. This is consistent with our Al-in-hornblende barometry results which suggest that sample TAJ93 was emplaced at depths of 7–9 km (~1.9–2.5 Kb). The ~160 Ma zircon (U/Th)-He ages in the southern part of the lake imply that cooling continued at a rate of ~4 to 8°C/Ma between ~203–160 Ma, likely as the plutons came into equilibrium with the regional thermal gradient. Based on the difference between (U/Th)-He ages in coexisting apatite and zircon in samples from the southern transects, the Karakul granites then experienced a long period of extremely slow cooling (~0.7–1.1°C/Myr) and exhumation (0.035–0.04 mm/yr) between ~160–50 Ma. The Mesozoic history of the Karakul granites thus appears to be characterized by shallow emplacement and a long period of stability in the upper crust above the ~150°C isotherm.

[21] Constraints on the Cenozoic time-temperature history derived from modeling using the HeFTy program are presented in Figure 6 and discussed below [*Ketcham*, 2005]. Our data suggest that the rate of cooling increased significantly at ~50–40 Ma. One piece of evidence for this interpretation is the paired zircon (~165–150 Ma) and apatite (~45–38 Ma) ages from rocks in the southern part of the lake. Taken alone, these paired ages (samples p917-1, P916-1, p916-3, and p916-4) could be explained by a constant cooling rate of ~0.7°C/Ma beginning around 160 Ma (after closure of zircon) and continuing until today.

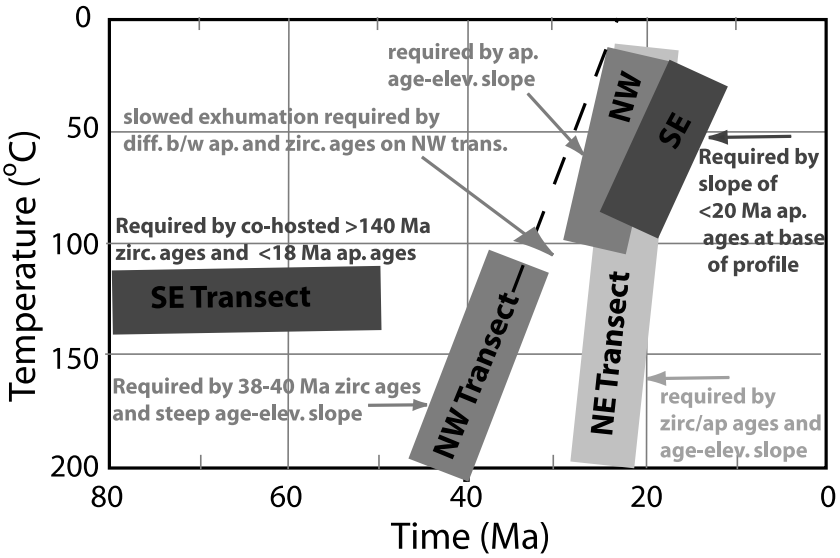

Figure 6. Constraints on thermal histories of the NW, NE, and SE profiles derived from thermal modeling using the HeFTy program [*Ketcham*, 2005]. The gray boxes reflect the possible thermal histories for each profile given the 1σ uncertainties of the measured ages, assumed thermal gradients, and assumed diffusion parameters. Dashed line denotes the projected cooling path for the NW profile, deviation from which implies a period of slowed exhumation between ~40 and 25 Ma. Text in the panel explains the major constraints on the cooling history of each profile.

However, this solution is unlikely based on the additional constraint provided by the zircon ages in the NW transect, which indicate a more rapid cooling rate of ~14 ± 5°C a^{-1} (~0.55 ± 0.20 mm/yr) from 40 to 38 Ma (Figure 4). If we assume that this reflects the regional cooling rate at this time, and therefore apply it to samples from the southern part of the lake, it requires a thermal history in which there is a period of very slow cooling (<0.5°C a^{-1}) until at least 55–50 Ma, followed by a shift to more rapid cooling. Applying this cooling rate over 30–40 km spatial scales is reasonable because it reflects cooling of samples at 6–9 km depth, where the effect of differential surface erosion rate on cooling at depth is greatly damped [*Reiners*, 2007]. An acceleration in cooling and exhumation rates at ~50–40 Ma is consistent with the possible break in slope observed in the SW apatite He age profile, suggesting that the highest sample in the SW profile may be the bottom of an exhumed partial retention zone (Figure 4).

[22] Sometime after ~40 Ma the average rate of exhumation must have slowed throughout the region. If exhumation had continued from 40 Ma onward at the rate of 0.55 mm/yr, or even at the 1σ lower bound of 0.25 mm/yr, we would expect <50 Ma zircon ages to have been exhumed in the southern part of the basin. Instead, the youngest observed zircon age is ~135 Ma. Exhumation also appears to have slowed to a lesser degree along the NW profile sometime after 40 Ma (dashed line in Figure 6). Time-temperature age modeling using the HeFTy program indicates that if exhumation had been proceeding at 0.55 mm/yr at 40 Ma, it would need to slow to a linear rate of ~0.05 mm/yr shortly thereafter to produce the 20–18 Ma apatite cooling ages observed in the same samples. If it had been proceeding at the 1σ lower rate of 0.25 mm/yr, it would need to slow slightly to ~0.2 mm/yr. Likewise, the rate of exhumation of the northern half of the lake basin cannot have exceeded an average rate of ~0.15 mm/yr since ~18 Ma without bringing even younger apatite cooling ages to the surface at the base of the NW and NE transects.

[23] The overall decrease in cooling rate after ~40 Ma rate conflicts with the steep age-elevation relationships observed in the NE and NW transects between ~25–16 Ma. Apatite ages from the NW transect imply an exhumation rate of >0.5 mm/yr from ~20–18 Ma (Figures 2 and 4). The apatite age-elevation transect from the NE profile indicates an exhumation rate >0.6 mm/yr between 19 and 17 Ma. Additionally, time-temperature age modeling of paired apatite and zircon cooling ages in sample TAJ99 and TAJ102 from the NE transect suggest that exhumation rates reached ~0.8 mm/yr between ~22–15 Ma [*Ketcham*, 2005]. The simplest thermal history that satisfies all of the above constraints is one in which a relatively slow Cenozoic cooling rate is punctuated by two periods of accelerated exhumation at ~50–40 Ma and ~25–16 Ma.

6. Discussion

6.1. Eocene Cooling

[24] Apatite and zircon (U/Th)-He ages record a period of accelerated exhumation at ~50–40 Ma. We speculate that this period of accelerated exhumation was an erosional response to tectonic uplift driven by India-Asia collision. This timing is similar to the onset of thrusting, exhumation, and basin filling documented along more easterly parts of the Tibet-Tarim margin; the Qimen Tagh and North Qaidam

thrust at ~49 Ma, the Hoh-Xil basin at ~49 Ma, and the Qaidam foreland at ~46 Ma [*Yin et al.*, 2002; *Zhu et al.*, 2006]. Slightly younger initiation age estimates have also been published for the Qaidam region; ~43 Ma basin based on restoration of balanced cross sections [*Zhou et al.*, 2006], and ~40 +/− 10 Ma based fission track ages in thrust-fault hanging walls [*Jolivet et al.*, 2001].

[25] In contrast to northeastern Tibet, relatively little evidence exists for tectonic activity in the Pamir and southern Tien Shan during Eocene time. The sedimentary record in the Tajik depression records shallow marine conditions during the Eocene with little or no preservation of syntectonic clastic successions at this time [*Burtman*, 2000; *Coutand et al.*, 2002; *Hamburger et al.*, 1992; *Leith*, 1985]. It is not clear whether the general lack of Eocene syntectonic deposits can be taken as evidence of tectonic quiescence, or whether proximal sediments were deposited far to the south and subsequently destroyed by northward overthrusting of the Pamir salient. One well preserved section of Cretaceous-Neogene sediments has been studied at Aertashi and nearby Puska, where a variety of evidence suggests that the western Kunlun fault system was active by ~46 Ma [*Yin et al.*, 2002]. This inference is supported by the large number of ~65–40 Ma detrital fission track ages from Paleogene sediments at the Aertashi site [*Sobel and Dumitru*, 1997]. These detrital ages are primarily from shallow marine or distal fluvial sediments that were transported from the south, and may have lag times (cooling age minus depositional age) as little as ~10 Ma. These detrital apatites were probably derived from some portion of the Northern Kunlun or Karakul-Mazar-Songpan terranes that experienced tectonic uplift and denudation during the Eocene in response to India-Asia collision. Given the similarity in cooling ages, the Karakul region may be analogous to the source terrane for the Paleogene Aertashi sediments. The Karakul region experienced so little subsequent Cenozoic exhumation that Eocene cooling ages are still present in the bedrock today. Today, the Karakul block sits north of Aertashi due to northward translation by the Karakoram and/or Kashar/Yecheng fault systems [*Cowgill*, 2010; *Robinson*, 2009].

[26] In summary, accelerated cooling between ~50–40 Ma provides an additional argument that localized tectonic uplift was occurring along the western end of the Tibet-Tarim margin within ~10 Ma of India-Asia collision. This adds to the growing body of evidence suggesting that the forces associated with India-Asia collision were transmitted very rapidly from south to north, driving deformation along the Tarim margin soon after India-Asia collision. Although this contrasts with both rigid block [*Tapponnier et al.*, 2001] and viscous sheet [*England and Houseman*, 1986] models of deformation that have been previously proposed, it is in agreement with recent numerical calculations showing that such far-field lithospheric deformation is possible shortly after collision [*Dayem et al.*, 2009].

6.2. Oligo-Miocene Cooling

[27] We consider two end-member explanations for the second phase of accelerated exhumation between 25 and 16 Ma: (1) accelerated exhumation throughout the eastern Pamir plateau in response to regional uplift or (2) the onset of localized extensional faulting within the Karakul graben at this time. As discussed below we favor the regional exhumation model based on the compelling coincidence of the 25–16 Ma (U/Th)-He ages observed at Karakul with $^{40}Ar/^{39}Ar$ and fission track ages observed throughout the region. This model implies that localized extensional faulting occurred sometime after the early Miocene, perhaps synchronous with the onset of east-west extension along the Kongur Shan and Muztagh-Ata fault systems at 8–7 Ma [*Robinson et al.*, 2004]. Accordingly, we infer that the magnitude of extension at Karakul has not been great enough to exhume apatite (U/Th)-He ages related to active extension.

[28] Any regional tectonic model invoked to explain exhumation at Karakul should also explain bedrock cooling ages of similar early Miocene age throughout the region. For example, $^{40}Ar/^{39}Ar$ ages and apatite/zircon fission track ages for the Sares and Muzkol domes in the central Pamir cluster almost entirely within a range of 23–14 Ma [*Schmalholz*, 2004]. Recent results from muscovite $^{40}Ar/^{39}Ar$ ages in rivers draining the interior of the eastern Pamir show strikingly narrow detrital age distributions, which are centered at ~18 Ma [*Lukens et al.*, 2009]. In the southern Pamir, hornblende and biotite $^{40}Ar/^{39}Ar$ ages from the Goran metamorphic series cluster between 22 and 17 Ma, likely recording exhumation at that time [*Hubbard et al.*, 1999]. In the western Kunlun, the Kudi quartz monzonite records zircon and apatite fission track ages of ~22 Ma and ~17 Ma, respectively [*Arnaud*, 1992].

[29] Whereas bedrock cooling ages generally indicate exhumation throughout the region, stratigraphic evidence points specifically to renewed thrusting and accelerated clastic sedimentation along the Main Pamir Thrust (MPT) during the early Miocene. For example, basin subsidence curves constructed for the Tajik depression along the western flank of the Pamir show the onset of rapid subsidence at ~22 Ma, likely in response to tectonic loading [*Leith*, 1985]. On the eastern flank of the Pamir, accelerated tectonic convergence is recorded at 22–17 Ma by reset apatite fission track ages in basin sediments exhumed near the foot of the MPT [*Sobel and Dumitru*, 1997]. Likewise, *Coutand et al.* [2002] observe a sharp increase in the deposition of terrestrial clastic sediments in the Alai valley sometime in the late Oligocene or early Miocene. Finally, basinal sediments throughout the southern Tien Shan contain apatite fission track ages of ~25–16 Ma that record accelerated exhumation, presumably related to the onset of thrust faulting [*Sobel and Dumitru*, 1997; *Sobel et al.*, 2006].

[30] Along the MPT and throughout the southern Tien Shan, early Miocene cooling ages can be directly linked to thrust-driven exhumation. Renewed activity along these more northerly thrust margins likely reflects a major change in the regional stress distribution of the India-Asia deformation zone. However, the observed exhumation of the Karakul granitoids, the Sares-Muzkol gneisses, and the Goran schists during the early Miocene is difficult to attribute to thrusting because none of the sites are known to sit in the hanging wall of major thrusts. We suggest that early

Miocene cooling ages within the interior of the Pamir may instead record unroofing in response to accelerated regional uplift of the entire Pamir plateau.

[31] A large-scale tectonic mechanism is attractive, and perhaps required, to explain the widespread renewal of tectonic uplift and denudation throughout the Pamir during the early Miocene. One possible mechanism for regional uplift without upper crustal thrusting comes from *Robinson et al.* [2007], who propose that crustal thickening occurred by under plating of material beneath the Pamir along a regional décollement (the eastern Pamir shear zone) during the late Oligocene and Miocene. Under this model, thickening of lower crust eventually leads to partial melting and extrusion of the central Pamir gneiss domes. This idea is attractive because it allows for diachronous extrusion, explaining why the Muzkol and Sares gneiss domes were being rapidly exhumed during the early Miocene, while the Muztag-Ata dome was apparently still undergoing prograde metamorphism. Although not mentioned in the model of *Robinson et al.* [2007], regional thickening of the lower crust could drive isostatic uplift of the plateau. We thus suggest that the onset of rapid exhumation at Karakul at ~25 Ma could be a response to uplift associated with the Oligo-Miocene crustal thickening inferred by *Robinson et al.* [2007].

[32] Here we present two possible tectonic scenarios to explain the onset of thickening and/or uplift at ~25 Ma. One idea is that uplift was driven by a second slab break off event along the down-going Indian plate at ~25 Ma [*Mahéo et al.*, 2002, 2009]. This event is inferred from the emplacement of ~24–22 Ma lamprophyres which are highly enriched in large ion lithophile elements thought to be derived from melting of metasomatized mantle. The simplest way to produce such compositions, as well as the observed advective thermal anomaly, is to induce a tear in the down-going slab, allowing fresh asthenosphere to rise through the newly created gap and melt the metasomatized mantle lithosphere [*Mahéo et al.*, 2002]. A slab break off event would cause the buoyant leading edge of the Indian lithosphere to rise, transmitting a larger portion of India's collisional force directly northward to the Pamir and Tien Shan. Some of this force would be transmitted through the rigid upper crust causing renewed thrusting along the MPT, whereas some would drive viscous deformation and thickening of the lower crust. A second and not necessarily exclusive idea is that development of the Karakoram fault during the early Miocene accelerated the northward translation of the Karakoram and southern Pamir blocks [*Lacassin et al.*, 2004; *Valli et al.*, 2008]. In the upper crust, this northward translation could have been accommodated by thrusting within the Rushan-Pshart zone. A regional décollement (the eastern Pamir shear zone) would allow the less viscous lower crust to bypass the Rushan-Pshart zone, thickening the crust below the Muzkol and Sares domes, as well as below the Karakul region. Because Muztagh-Ata sits on the opposite side of the Karakoram fault, the flux of material and rate of crustal thickening would be less, ultimately delaying extrusion of the gneiss dome until the late Miocene.

6.3. Implications for the Timing of Extension at Karakul

[33] In the above interpretation, the Karakul region would have experienced uplift and erosion as part of a hinterland plateau structurally above and behind the Main Pamir Thrust. Rocks at the surface today would have been exhumed through their closure isotherm during the early Miocene and then remained at depths of <~3 km until being exhumed by extensional faulting sometime after ~16 Ma. This interpretation is consistent with observations from the nearby Kongur Shan fault system which does not record the onset of east–west extension until ~8–7 Ma [*Robinson et al.*, 2004]. However, no <16 Ma apatite (U/Th)-He ages are observed at Karakul that document the exhumation of a late Miocene–Pliocene partial annealing zone via extensional faulting. This lack of young ages probably reflects the fact that the total exhumation of the footwall is not enough to have exhumed a late Miocene or Pliocene partial annealing zone. This observation can be used to place lower bounds on the total amount of extension accommodated by structures bounding the Karakul graben. To explore these constraints we calculate that given a geothermal gradient of 25°C/km and a 65°C closure temperature, a fault would require ~2.5 km of vertical throw to exhume the top of the apatite (U/Th)-He partial annealing zone. Adopting a fault dip of 60°, and recognizing that 2.5 km of vertical offset has not been achieved requires that less than 1.5 km of horizontal extension has accumulated across any of the bounding normal faults. If the majority of extension is focused along the two bounding faults along the eastern and western flanks, then the total extension across the basin may not have exceeded ~3 km. Acknowledging these constraints, and adopting a range of horizontal extension rates from 0.5 to 1 mm/yr (see above), implies that extension may have begun between ~9–3 Ma.

[34] It appears that our data are insufficient to constrain the exact timing of extensional faulting within the Karakul graben and highlight the differences in total extension and exhumation between the Karakul and Kongur Shan systems. The possibility of temporal and/or mechanical linkage between these extensional systems remains an outstanding question and differences in the magnitude of exhumation further obfuscates the problem. Future work applying $^{3}He/^{4}He$ thermochronology may better constrain the timing and magnitude of extension at Karakul and address potential causes of extension in the eastern Pamir [*Shuster and Farley*, 2004].

6.4. Bulk Geochemistry Data

[35] The geochemical data presented in section 4 are consistent with the idea of *Schwab et al.* [2004] that the Karakul granitoids are correlated with the Mazar granitoids of the western Kunlun. This correlation suggests that the Kunlun suture is a continuous feature which wraps around the Pamir salient and that the total tectonic offset along the Karakoram fault is moderate [*Robinson*, 2009; *Schwab et al.*, 2004]. The Karakul granites have a fundamentally arc-type composition, reflecting a relatively mature arc source and little contribution from intraplate melting. The relatively

consistent geochemical signature observed in each of the three profiles suggests that the Karakul granitoids were emplaced as a large volume plutonic system, which has not experienced significant reheating or tectonic deformation. Collectively, these observations imply that the Karakul region has behaved as a rigid block of crust during Cenozoic tectonism, akin to the Sierra Nevada batholith of the western United States. The existence of pull-apart basin within an apparently contiguous batholith suggests that extension at Karakul may be due to the interplay of well developed regional fault systems, rather than inherent weakness in the upper crust near Karakul.

7. Conclusions

[36] We present new apatite and zircon (U/Th)-He ages, Al in hornblende barometry, and bulk rock geochemical data from granitoid rocks flanking the Karakul graben. Bulk rock geochemistry of the Karakul granitoids is similar to the data published by *Schwab et al.* [2004], further supporting their inference that the Karakul granitoids are correlated with the Mazar granites and that the northern Pamir terrane is a continuation of the Songpan-Garze terrane. When considered in the context of existing geochronology [*Schwab et al.*, 2004], our Al in hornblende barometry results show that the Karakul granitoids were emplaced at shallow depths (~7–9 km), and cooled quickly through ~300°C. Initially rapid cooling was followed by a prolonged period of relatively slow cooling between ~190 and 50 Ma. Based on a steep Eocene age-elevation profile, and a second profile containing a possible break in slope near 50 Ma, we conclude that a period of accelerated cooling and exhumation began sometime between ~50–40 Ma. We speculate that this period of cooling reflects an erosional response to far-field tectonic uplift associated with the India-Asia collision. This lends support to the idea that tectonic shear and strain were transmitted to the northwestern Tarim margin within ~10 Ma of India-Asia collision [*Dayem et al.*, 2009; *Yin et al.*, 2008]. Based on steep early Miocene age-elevation profiles and a pronounced break in age-elevation slope near ~25–20 Ma, we infer a period of accelerated exhumation between ~25–16 Ma. The widespread occurrence of 25–16 Ma cooling ages elsewhere in the region suggests that this early Miocene period of exhumation is part of a renewed phase of plateau uplift driven by regional tectonism sometime ~25–22 Ma. This renewed tectonism in the northern Pamir may have resulted from break off of the down-going Indian slab at ~25 Ma, development of the Karakoram fault system, or both.

[37] **Acknowledgments.** We would like to thank Mars Toktogonov, Kanatbek Abdrakhmatov, and Anatoli Ischuk for help with planning and logistics. This project would not have been possible without funding from the Geological Society of America Structural Geology and Tectonics division, the California Mineralogical Society, and Sigma Xi. Thanks to Ken Farley for advice on data analysis and for the use of his lab. We also thank Alex Robinson, Ed Sobel, Rasmus Thiede, and the *Tectonics* editorial staff for detailed reviews that greatly improved this manuscript in every regard.

References

Arnaud, N. (1992), *Apport de la Thermochronologie $^{40}Ar/^{39}Ar$ sur Feldspath Potassique a la Connaissance de la Tectonique Cenozoique d'Asie*, Univ. Blaise Pascal, Clermont-Ferrand II, Clermont-Ferrand, France.

Arrowsmith, J. R., and M. R. Strecker (1999), Seismotectonic range-front segmentation and mountain-belt growth in the Pamir-Alai region, Kyrgyzstan (India-Eurasia collision zone), *Geol. Soc. Am. Bull.*, *111*(11), 1665–1683, doi:10.1130/0016-7606(1999)111<1665:SRFSAM>2.3.CO;2.

Beloussov, V. V., et al. (1980), Structure of the lithosphere along the deep seismic-sounding profile—Tien Shan-Pamirs-Karakorum-Himalayas, *Tectonophysics*, *70*(3–4), 193–221, doi:10.1016/0040-1951(80)90279-6.

Blisniuk, P. M., and M. R. Strecker (1996), Kinematics of Holocene normal faulting in the northern Pamir, *Eos Trans. AGU*, *77*(46), Fall Meet. Suppl., Abstract T21B-14.

Blisniuk, P. M., and M. R. Strecker (1997), Quaternary oblique normal faulting in the Lake Karakul area, northern Pamir (Tajikistan): Transfer of lateral escape along the Karakorum and Altyn Tagh faults?, *Geol. Soc. Am. Abstr. Programs*, *29*(6), 470.

Brunel, M., N. Arnaud, P. Tapponnier, Y. Pan, and Y. Wang (1994), Kongur Shan normal fault: Type example of mountain building assisted by extension (Karakoram fault, eastern Pamir), *Geology*, *22*(8), 707–710, doi:10.1130/0091-7613(1994)022<0707:KSNFTE>2.3.CO;2.

Burtman, V. S. (2000), Cenozoic crustal shortening between the Pamir and Tien Shan and a reconstruction of the Pamir-Tien Shan transition zone for the Cretaceous and Palaeogene, *Tectonophysics*, *319*(2), 69–92, doi:10.1016/S0040-1951(00)00022-6.

Burtman, V. S., and P. Molnar (1993), Geological and geophysical evidence for deep subduction beneath the Pamir, *Spec. Pap. Geol. Soc. Am.*, *281*, 1–76.

Clark, M. K., and L. H. Royden (2000), Topographic ooze: Building the eastern margin of Tibet by lower crustal flow, *Geology*, *28*(8), 703–706, doi:10.1130/0091-7613(2000)28<703:TOBTEM>2.0.CO;2.

Coutand, I., M. R. Strecker, J. R. Arrowsmith, G. Hilley, R. C. Thiede, A. Korjenkov, and M. Omuraliev (2002), Late Cenozoic tectonic development of the intramontane Alai Valley, (Pamir-Tien Shan region, central Asia): An example of intracontinental deformation due to the Indo-Eurasia collision, *Tectonics*, *21*(6), 1053, doi:10.1029/2002TC001358.

Cowgill, E. (2010), Cenozoic right-slip faulting along the eastern margin of the Pamir salient, northwestern China, *Geol. Soc. Am. Bull.*, *122*(1–2), 145–161, doi:10.1130/B26520.1.

Dayem, K. E., P. Molnar, M. K. Clark, and G. A. Houseman (2009), Far-field lithospheric deformation in Tibet during continental collision, *Tectonics*, *28*, TC6005, doi:10.1029/2008TC002344.

Ehlers, T. A., and K. A. Farley (2003), Apatite (U-Th)/He thermochronometry: Methods and applications to problems in tectonic and surface processes, *Earth Planet. Sci. Lett.*, *206*(1–2), 1–14, doi:10.1016/S0012-821X(02)01069-5.

England, P., and G. Houseman (1986), Finite strain calculations of continental deformation: 2. Comparison with the India-Asia collision zone, *J. Geophys. Res.*, *91*(B3), 3664–3676, doi:10.1029/JB091iB03p03664.

Farley, K. A. (2000), Helium diffusion from apatite: General behavior as illustrated by Durango fluorapatite, *J. Geophys. Res.*, *105*(B2), 2903–2914, doi:10.1029/1999JB900348.

Farley, K. A. (2002), (U-Th)/He dating: Techniques, calibrations, and applications, in *Noble Gases in Geochemistry and Cosmochemistry*, edited by D. Porcelli, C. J. Ballentine, and R. Wieler, pp. 819–844, Geochem. Soc., Columbus, Ohio.

Farley, K. A., et al. (1996), The effects of long alpha-stopping distances on (U-Th)/He ages, *Geochim. Cosmochim. Acta*, *60*(21), 4223–4229.

Gurov, E. P., H. P. Gurova, R. B. Rakitskaya, and A. Y. Yamnichenko (1993), The Karakul depression in Pamirs: The first impact structure in central Asia, *Lunar Planet. Sci.*, *XXIV*, 591–592.

Hamburger, M. W., D. R. Sarewitz, T. L. Pavlis, and G. A. Popandopulo (1992), Structural and seismic evidence for intracontinental subduction in the Peter the First Range, central Asia, *Geol. Soc. Am. Bull.*, *104*(4), 397–408, doi:10.1130/0016-7606(1992)104<0397:SASEFI>2.3.CO;2.

Hammarstrom, J. M., and E. Zen (1986), Aluminum in hornblende: An empirical igneous geobarometer, *Am. Mineral.*, *71*, 1297–1313.

Hollister, L. S., G. C. Grissom, E. K. Peters, H. H. Stowell, and V. B. Sisson (1987), Confirmation of the empirical correlation of Al in hornblende with pressure of solidification of calc-alkaline plutons, *Am. Mineral.*, *72*, 231–239.

House, M. A., K. A. Farley, and D. Stockli (2000), Helium chronometry of apatite and titanite using Nd-YAG laser heating, *Earth Planet. Sci. Lett.*, *183*(3–4), 365–368, doi:10.1016/S0012-821X(00)00286-7.

Hubbard, M. S., E. S. Grew, K. V. Hodges, M. G. Yates, and N. N. Pertsev (1999), Neogene cooling and exhumation of upper-amphibolite-facies 'whiteschists' in the southwest Pamir Mountains, Tajikistan, *Tectonophysics*, *305*(1–3), 325–337, doi:10.1016/S0040-1951(99)00012-8.

Jolivet, M., M. Brunel, D. Seward, Z. Xu, J. Yang, F. Roger, P. Tapponnier, J. Malavieille, N. Arnaud, and C. Wu (2001), Mesozoic and Cenozoic tectonics of the northern edge of the Tibetan plateau: Fission-track constraints, *Tectonophysics*, *343*(1–2), 111–134, doi:10.1016/S0040-1951(01)00196-2.

Ketcham, R. A. (2005), Forward and inverse modeling of low-temperature thermochronometry data, in *Low-Temperature Thermochronology: Techniques, Interpretations, and Applications*, edited by P. W. Reiners and T. A. Ehlers, pp. 275–314, Mineral. Soc. of Am., Chantilly, Va.

Kohn, M. J., and F. Spear (2000), Retrograde net transfer reaction insurance for pressure-temperature estimates, *Geology*, *28*(12), 1127–1130, doi:10.1130/0091-7613(2000)28<1127:RNTRIF>2.0.CO;2.

Komatsu, T., T. Watanabe, and K. Hirakawa (2010), A framework for Late Quaternary lake-level fluctuations in Lake Karakul, eastern Pamir, focusing on lake-glacier landform interaction, *Geomorphology*, *119*, 198–211, doi:10.1016/j.geomorph. 2010.03.025.

Lacassin, R., et al. (2004), Large-scale geometry, offset and kinematic evolution of the Karakorum fault, Tibet, *Earth Planet. Sci. Lett.*, *219*(3–4), 255–269, doi:10.1016/S0012-821X(04)00006-8.

Leith, W. (1985), A Mid-Mesozoic extension across central Asia, *Nature*, *313*(6003), 567–570, doi:10.1038/313567a0.

Lukens, C. E., B. Carrapa, L. M. Schoenbohm, B. S. Singer, and B. Jicha (2009), Tectono-thermal evolution of the western Pamir Mountains, using $^{40}Ar/^{39}Ar$ thermochronology on modern river sands, *Eos Trans. AGU*, *90*(52), Fall Meet. Suppl., Abstract T43C-2099.

Mahéo, G., S. Guillot, J. Blichert-Toft, Y. Rolland, and A. Pêcher (2002), A slab breakoff model for the Neogene thermal evolution of South Karakorum and South Tibet, *Earth Planet. Sci. Lett.*, *195*(1–2), 45–58, doi:10.1016/S0012-821X(01)00578-7.

Mahéo, G., J. Blichert-Toft, C. Pin, S. Guillot, and A. Pêcher (2009), Partial melting of mantle and crustal sources beneath South Karakorum, Pakistan: Implications for the Miocene geodynamic evolution of the India-Asia Convergence Zone, *J. Petrol.*, *50*(3), 427–449, doi:10.1093/petrology/egp006.

Matte, P., et al. (1996), Tectonics of western Tibet, between the Tarim and the Indus, *Earth Planet. Sci. Lett.*, *142*(3–4), 311–330.

Murphy, M. A., A. Yin, P. Kapp, T. M. Harrison, D. Lin, and J. H. Guo (2000), Southward propagation of the Karakoram fault system, southwest Tibet: Timing and magnitude of slip, *Geology*, *28*(5), 451–454, doi:10.1130/0091-7613(2000)28<451:SPOTKF>2.0.CO;2.

Noth, L. (1932), *Geologische Untersuchungen im Nordwestlichen Pamir-Gebiet und Mittleren Trans-Alai*, 204 pp., Reimer-Vohsen, Berlin.

Peltzer, G., and P. Tapponnier (1988), Formation and evolution of strike-slip faults, rifts, and basins during the India-Asia collision: An experimental approach, *J. Geophys. Res.*, *93*(B12), 15,085–15,117, doi:10.1029/JB093iB12p15085.

Phillips, R. J., R. R. Parrish, and M. P. Searle (2004), Age constraints on ductile deformation and long-term slip rates along the Karakoram fault zone, Ladakh, *Earth Planet. Sci. Lett.*, *226*(3–4), 305–319, doi:10.1016/j.epsl.2004.07.037.

Raterman, N. S., et al. (2007), Variable structural style along the Karakoram fault explained using triple-junction analysis of intersecting faults, *Geosphere*, *3*, 71–85.

Reigber, C., G. W. Michel, R. Galas, D. Angermann, J. Klotz, J. Y. Chen, A. Papschev, R. Arslanov, V. E. Tzurkov, and M. C. Ishanov (2001), New space geodetic constraints on the distribution of deformation in central Asia, *Earth Planet. Sci. Lett.*, *191*(1–2), 157–165, doi:10.1016/S0012-821X(01)00414-9.

Reiners, P. W. (2007), Thermochronologic approaches to paleotopography, in *Paleoaltimetry: Geochemical and Thermodynamic Approaches*, edited by M. J. Kohn, pp. 243 −267, Mineral. Soc. of Am., Chantilly, Va.

Reiners, P. W., K. A. Farley, and H. J. Hickes (2002), He diffusion and (U-Th)/He thermochronometry of zircon: Initial results from Fish Canyon Tuff and Gold Butte, *Tectonophysics*, *349*(1–4), 297–308, doi:10.1016/S0040-1951(02)00058-6.

Reiners, P. W., T. L. Spell, S. Nicolescu, and K. A. Zanetti (2004), Zircon (U-Th)/He thermochronometry: He diffusion and comparisons with $^{40}Ar/^{39}Ar$ dating, *Geochim. Cosmochim. Acta*, *68*(8), 1857–1887, doi:10.1016/j.gca.2003.10.021.

Renne, P. R., A. L. Deino, R. C. Walter, B. D. Turrin, C. C. Swisher III, T. A. Becker, G. H. Curtis, W. D. Sharp, and A.-R. Jaouni (1994), Intercalibration of astronomical and radioisotopic time, *Geology*, *22*(9), 783–786, doi:10.1130/0091-7613(1994)022<0783:IOAART>2.3.CO;2.

Robinson, A. C. (2009), Geologic offsets across the northern Karakorum fault: Implications for its role and terrane correlations in the western Himalayan-Tibetan orogen, *Earth Planet. Sci. Lett.*, *279*(1–2), 123–130, doi:10.1016/j.epsl.2008.12.039.

Robinson, A. C., A. Yin, C. E. Manning, T. M. Harrison, S.-H. Zhang, and X.-F. Wang (2004), Tectonic evolution of the northeastern Pamir: Constraints from the northern portion of the Cenozoic Kongur Shan extensional system, western China, *Geol. Soc. Am. Bull.*, *116*(7–8), 953–973, doi:10.1130/B25375.1.

Robinson, A. C., A. Yin, C. E. Manning, T. M. Harrison, S.-H. Zhang, and X.-F. Wang (2007), Cenozoic evolution of the eastern Pamir: Implications for strain-accommodation mechanisms at the western end of the Himalayan-Tibetan orogen, *Geol. Soc. Am. Bull.*, *119*(7–8), 882–896, doi:10.1130/B25981.1.

Romanko, E. (1968), Geological map of the Tadjik SSR, sheet J-43-XIII, scale 1:200,000, Russ. Geol. Minist., St. Petersburg, Russia.

Schmalholz, M. (2004), *The Amalgamation of the Pamirs and Their Subsequent Evolution in the Far Field of the India-Asia Collision*, 185 pp., Univ. of Tübingen, Tübingen, Germany.

Schwab, M., L. Ratschbacher, and W. Frisch (1999), Cenozoic to recent thermodynamic evolution of S-Tien Shan, NE- and central Pamirs: Evidences from U/Pb, $^{40}Ar/^{39}Ar$ and fission-track dating methods combined with structural analyses, *J. Conf. Abstr.*, *4*(1), 54.

Schwab, M., et al. (2004), Assembly of the Pamirs: Age and origin of magmatic belts from the southern Tien Shan to the southern Pamirs and their relation to Tibet, *Tectonics*, *23*, TC4002, doi:10.1029/2003TC001583.

Searle, M. P. (1996), Geological evidence against large-scale pre-Holocene offsets along the Karakoram Fault: Implications for the limited extrusion of the Tibetan plateau, *Tectonics*, *15*(1), 171–186.

Shuster, D. L., and K. A. Farley (2004), $^{4}He/^{3}He$ thermochronometry, *Earth Planet. Sci. Lett.*, *217*(1–2), 1–17, doi:10.1016/S0012-821X(03)00595-8.

Sobel, E. R., and T. A. Dumitru (1997), Thrusting and exhumation around the margins of the western Tarim basin during the India-Asia collision, *J. Geophys. Res.*, *102*(B3), 5043–5063, doi:10.1029/96JB03267.

Sobel, E. R., J. Chen, and R. V. Heermance (2006), Late Oligocene-Early Miocene initiation of shortening in the southwestern Chinese Tian Shan: Implications for Neogene shortening rate variations, *Earth Planet. Sci. Lett.*, *247*(1–2), 70–81, doi:10.1016/j.epsl.2006.03.048.

Stockli, D. F., T. A. Dumitru, M. O. McWilliams, and K. A. Farley (2003), Cenozoic tectonic evolution of the White Mountains, California and Nevada, *Geol. Soc. Am. Bull.*, *115*(7), 788–816, doi:10.1130/0016-7606(2003)115<0788:CTEOTW>2.0.CO;2.

Strecker, M. R., W. Frisch, M. W. Hamburger, L. Ratschbacher, S. Semiletkin, A. Samoruyev, and N. Sturchio (1995), Quaternary deformation in the Eastern Pamirs, Tadzhikistan and Kyrgyzstan, *Tectonics*, *14*(5), 1061–1079, doi:10.1029/95TC00927.

Strecker, M. R., G. E. Hilley, J. R. Arrowsmith, and I. Coutand (2003), Differential structural and geomorphic mountain-front evolution in an active continental collision zone: The northwest Pamir, southern Kyrgyzstan, *Geol. Soc. Am. Bull.*, *115*(2), 166–181, doi:10.1130/0016-7606(2003)115<0166:DSAGMF>2.0.CO;2.

Tapponnier, P., J. L. Mercier, R. Armijo, T. L. Han, and J. Zhou (1981), Field evidence for active normal faulting in Tibet, *Nature*, *294*(5840), 410–414, doi:10.1038/294410a0.

Tapponnier, P., Z. Q. Xu, F. Roger, B. Meyer, N. Arnaud, G. Wittlinger, and J. S. Yang (2001), Oblique stepwise rise and growth of the Tibet plateau, *Science*, *294*(5547), 1671–1677, doi:10.1126/science.105978.

Tindle, A., and P. Webb (1994), PROBE-AMPH—A spreadsheet program to classify microprobe-derived amphibole analyses, *Comput. Geosci.*, *20*(7–8), 1201–1228, doi:10.1016/0098-3004(94)90071-X.

Valli, F., et al. (2008), New U-Th/Pb constraints on timing of shearing and long-term slip-rate on the Karakorum fault, *Tectonics*, *27*, TC5007, doi:10.1029/2007TC002184.

Wang, E., F.-Y. Xu, J.-X. Zhou, J. Wan, and B. C. Burchfiel (2006), Eastward migration of the Qaidam basin and its implications for Cenozoic evolution of the Altyn Tagh fault and associated river systems, *Geol. Soc. Am. Bull.*, *118*(3–4), 349–365, doi:10.1130/B25778.1.

Yin, A., and T. M. Harrison (2000), Geologic evolution of the Himalayan-Tibetan orogen, *Annu. Rev. Earth Planet. Sci.*, *28*, 211–280, doi:10.1146/annurev.earth.28.1.211.

Yin, A., A. Robinson, and C. E. Manning (2001), Oroclinal bending and slab-break-off causing coeval east-west extension and east-west contraction in the Pamir-Nanga Parbat syntaxis in the past 10 m.y., *Eos Trans. AGU*, *82*(47), Fall Meet. Suppl., Abstract T12F-03.

Yin, A., et al. (2002), Tectonic history of the Altyn Tagh fault system in northern Tibet inferred from Cenozoic sedimentation, *Geol. Soc. Am. Bull.*, *114*(10), 1257–1295, doi:10.1130/0016-7606(2002)114<1257:THOTAT>2.0.CO;2.

Yin, A., Y.-Q. Dang, M. Zhang, X.-H. Chen, and M. W. McRivette (2008), Cenozoic tectonic evolution of the Qaidam basin and its surrounding regions (part 3): Structural geology, sedimentation, and regional tectonic reconstruction, *Geol. Soc. Am. Bull.*, *120*(7–8), 847–876, doi:10.1130/B26232.1.

Young, E., A. Myers, E. Munson, and N. Conklin (1969), Mineralogy and geochemistry of fluorapatite from Cerro de Mercado, Durango, Mexico, *U.S. Geol. Surv. Prof. Pap.*, *650-D*, 84–93.

Yuan, C., M. Sun, M. Zhou, H. Zhou, W. Xiao, and J. Li (2002), Tectonic evolution of the West Kunlun: Geochronologic and geochemical constraints from Kudi granitoids, *Int. Geol. Rev.*, *44*, 653–669, doi:10.2747/0020-6814.44.7.653.

Yuquan, Z., X. Yingwen, X. Ronghua, P. Vidal, and N. Arnaud (1996), Geochemistry of granitoid rocks, in *Geological Evolution of the Karakorum and Kunlun Mountains*, edited by P. Yusheng, pp. 132–168, Seismol. Press, Beijing.

Zhou, J. X., F. Y. Xu, T. C. Wang, A. F. Cao, and C. M. Yin (2006), Cenozoic deformation history of the Qaidam Basin, NW China: Results from cross-section restoration and implications for Qinghai-Tibet Plateau tectonics, *Earth Planet. Sci. Lett.*, *243*(1–2), 195–210, doi:10.1016/j.epsl.2005.11.033.

Zhu, L. D., C. S. Wang, H. B. Zheng, F. Xiang, H. S. Yi, and D. Z. Liu (2006), Tectonic and sedimentary evolution of basins in the northeast of Qinghai-Tibet Plateau and their implication for the northward growth of the plateau, *Palaeogeogr. Palaeoclimatol. Palaeoecol.*, *241*(1), 49–60, doi:10.1016/j.palaeo.2006.06.019.

W. H. Amidon, Department of Geology, Middlebury College, Middlebury, VT 05753, USA. (wamidon@gps.caltech.edu)

Scott A. Hynek, Department of Geology and Geophysics, University of Utah, Salt Lake City, UT 84112, USA.